

Article

Magnetic Interaction in Doped 2D Perovskite Cuprates with Nanoscale Inhomogeneity: Lattice Nonlocal Effects vs. Superexchange

Vladimir A. Gavrichkov *  and Semyon I. Polukeev

Kirensky Institute of Physics, Akademgorodok 50, building 38, 660036 Krasnoyarsk, Russia

* Correspondence: gav@iph.krasn.ru

Abstract: We have studied the superexchange interaction J_{ij} in doped 2D cuprates. The AFM interaction strongly depends on the state of the lattice of a CuO_2 layer surrounded by two LaO rock salt layers. In a static U and D stripe nanostructure, the homogeneous AFM interaction is impossible due to the $U/D/U \dots$ periodic stripe sequence and $T_N = 0$. In a dynamic stripe nanostructure, the ideal CuO_2 layer with nonlocal effects and the homogeneous AFM interaction are restored. However, the interaction J_{ij} decreases by the exponential factor due to partial dynamic quenching. The meaning of the transition from the dynamic to the static cases lies in the spontaneous θ -symmetry breaking with respect to the rotation of all the tilted CuO_6 octahedra by an orientation angle $\delta\theta = n \cdot (45^\circ)$ (where $n = 1 \div 4$) in the U and D stripe nanostructure of the CuO_2 layer. Moreover, the structural features help to study various experimental data on the charge inhomogeneity, Fermi level pinning in the p type cuprates only and time reversal symmetry breaking from a unified point of view.

Keywords: superexchange interaction; nanoscale inhomogeneity; doped 2D perovskite cuprates



Citation: Gavrichkov, V.A.; Polukeev, S.I. Magnetic Interaction in Doped 2D Perovskite Cuprates with Nanoscale Inhomogeneity: Lattice Nonlocal Effects vs. Superexchange. *Condens. Matter* **2022**, *7*, 57. <https://doi.org/10.3390/condmat7040057>

Academic Editor: Antonio Bianconi

Received: 20 September 2022

Accepted: 13 October 2022

Published: 18 October 2022

Publisher's Note: MDPI stays neutral with regard to jurisdictional claims in published maps and institutional affiliations.



Copyright: © 2022 by the authors. Licensee MDPI, Basel, Switzerland. This article is an open access article distributed under the terms and conditions of the Creative Commons Attribution (CC BY) license (<https://creativecommons.org/licenses/by/4.0/>).

1. Introduction

The unique functionality of several materials with a perovskite structure, such as cuprates Refs. [1–4], can be tuned by atomic substitutions, tolerance factor, misfit strain and pressure, which control structural tilts and nanoscale phase separation. The scanning tunneling microscopy and spectroscopy (STM and STS) [5–9] and advanced experimental X-ray methods [10–14] in a wide range of temperature and doping unambiguously indicate that there is a clear connection between the multiscale stripe texture and the quantum coherence of quasiparticles in 2D perovskite high- T_c superconductors. The stripe charge nanostructure is also accompanied by spin inhomogeneity [15–23], and it is believed that high-temperature superconductivity (HTSC) originates from magnetic spin excitations that bind Cooper pairs [24–27]. The magnetic interaction in parent AFM 2D cuprates is the well-known superexchange interaction [28]. The AFM interaction between the nearest spins of Cu^{2+} ions in the CuO_2 layer is strong (~ 0.146 eV) [29], and it is much stronger than the interplanar exchange, which is mainly responsible for long-range magnetic ordering observed in undoped cuprates. For La_2CuO_4 (LCO), the Neel temperature is $T_N \approx 300$ K. In the traditional picture of BCS superconductivity, magnetism destroys Cooper pairs. However, superconductivity in these HTSCs develops from a “bad metal”, whose resistivity is higher than that of BCS superconductors, and the AFM magnetism itself is related to the initial “bad metal” state, where superconductivity occurs when long-range magnetic ordering is suppressed at a relatively weak hole doping ($x \sim 0.01$). Indeed, in the resonating-valence bond (RVB) approach and $t - J$ model [24,30–33], HTSC emerges due to the condensation of hole pairs, induced by the exchange interaction J_{ij} . Pairing of holes in this mechanism is caused by the interband transfer of quasiparticles in the CuO_2 layer with short-range AFM ordering. Retardation effects for this mechanism are insignificant. Another view on the HTSC state in the cuprates (see for example [34,35]) is that AFM spin fluctuations become

particularly longer-ranged and soft at low hole doping. In fact, there is a resonant magnetic mode [36–38] within the HTSC phase, where the scenario of spin fluctuations represents the lowest bosonic mode relevant for the d-wave HTSC pairing in the energy range $\sim J_{ij}$.

If the magnetic interaction is a reliable candidate that can be used as a glue for holes [39], then how will it change in the inhomogeneous nanostructure of doped 2D cuprates? Actual research on the properties of a quantum spin liquid in the double perovskite oxides with the general formula of $A_2Me_2O_6$ [40–42] does not provide a direct answer to this question, since there is no anion substitution in the CuO_2 layer of HTSC cuprates. However, the dynamical charge and spin nanoinhomogeneities are identified and discussed in current neutron and STM experiments [43–46]. Based on the large isotope effect in high-Tc superconductors with the stripe nanostructure [47–49], here we study superexchange interaction taking into account the phonon nature of the stripe structure in high-Tc cuprates. It will be shown that the charge and spin nanoscale phase separation can be derived at least qualitatively in the lattice approach, and the homogeneous interaction J_{ij} is restored at a certain hole concentration corresponding to an equal-dimensional periodic stripe structure of a linear or chess type. Furthermore, this is a good reason to test your feelings in accordance with the opinion: “. . .there remains the nagging feeling that even if the basic pairing mechanism ultimately arises from the short-range antiferromagnetic correlations in the layer, some important ingredient may be missing from the theory we have described” (see the review [25]). In conclusion, we discuss the observable consequences from the lattice concept of the stripe nature.

2. Color Approach to Nanoscale Inhomogeneity and D and U Stripe Structure

We focus on the tilting effects as a required attribute of the observed stripes [50]. The idea of the color approach [51] is the identification of stripes due to the tilting effects (tilting of the CuO_6 octahedron as a whole). The fact is that different stripes differ not only in the hole concentration and spin, but in the type of nuclear configuration (see Figure 1).

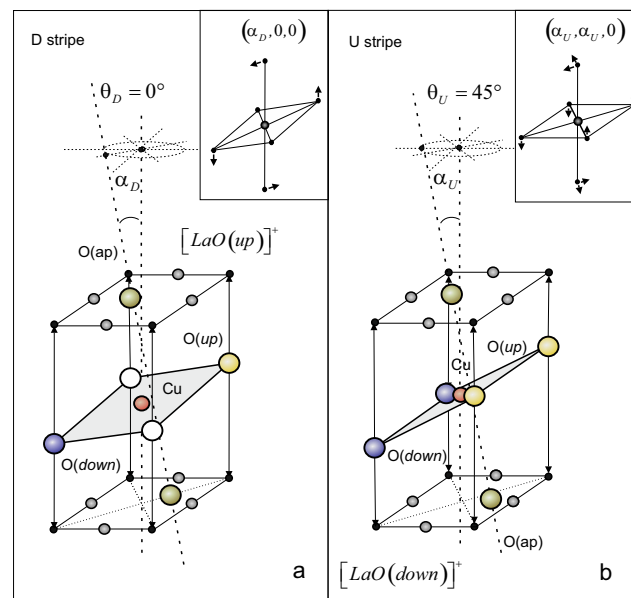


Figure 1. View of the tilted CuO_6 octahedra of the D (a) and U (b) stripes with different tilting effects in LSCO. The insets show the tilting effects in accordance with the Glazer’s notations [52].

We have classified the observed stripe configurations into a ninth-order symmetric Abelian group $G(\alpha)$ consisting of two types of stripes $U(\theta_U)$ and $D(\theta_D)$ rotated at the right angle relative to each other [51]. The sought stripe group $G(\alpha)$ represents all possible reaction products between different initial nuclear configurations in the form of group multiplication, where an ideal non-tilted prototype of the perovskite CuO_6 octahedron is used as a group unit. In all the “structural reactions” of nuclear configurations of the

stripes, the tilting angle α of the perovskite octahedron with respect to the rock salt LaO layers is retained, rather than their initial symmetry, as is the case, for example, of chemical reactions, in accordance with the Woodworth–Hoffman rules [53]. The number of nuclear configurations of the observed stripes in LSCO is reduced to one of the two $U(\theta_U)$ (where $\theta_U = 45^\circ, 135^\circ, 225^\circ, 315^\circ$) or $D(\theta_D)$ (where $\theta_D = 0^\circ, 90^\circ, 180^\circ, 270^\circ$) stripes, and their spatial distribution in the CuO_2 layer is represented by possible plane graphs with the chromatic number $\chi \leq 4$ in the four-color theorem. Using four colors: $U(45^\circ), U(225^\circ)$ —red (R), $U(135^\circ), U(315^\circ)$ —blue (B) and also $D(0^\circ), D(180^\circ)$ —green (G); $D(90^\circ), D(270^\circ)$ —yellow (Y), we can always color an arbitrary plane map, and the four colors R, G, B, Y are just four subgroups in $G(\alpha)$. The group can also be represented as a direct product of the subgroups of any different colors, e.g., $G(\alpha) = R \times B = G \times Y$, etc. The $D(\theta_D)$ stripes occur as overlapping different $U(\theta_U)$ and $U(\theta_U \pm 90^\circ)$ stripes in an $R/G/B$ sequence, for example, upon $U(\theta_U)$ stripes disordering with doping, and vice versa, $U(\theta_U)$ stripes can occur as overlapping $D(\theta_D)$ and $D(\theta_D \pm 90^\circ)$ stripes in the $G/R/Y$ sequence.

These two stripe sequences can be combined into one, for example into $Y/R/G/B$, from which, by rotating all the tilted CuO_6 octahedra around the c axis by the angle $\delta\theta = n \cdot (45^\circ)$, we can obtain other three $B/Y/R/G, G/B/Y/R$ and $R/G/B/Y$. The rotation also leads to a shift over the $G(\alpha)$ group and transverse shift of the linear stripe and diagonal shift of the checkerboard structures in Figure 2. This means that the ground state of the CuO_2 layer in Figure 2 is fourfold degenerate with respect to the rotation. Indeed, we can also form a novel JT cell (see Figure 2), and during its translation the number of hole carriers and spins in the JT cell is retained. The state Ψ_{θ_n} of the JT cell is fourfold degenerate by the initial phase $\theta_n = 0, 45^\circ, 90^\circ, 135^\circ$, which splits upon tunneling the CuO_6 octahedra over the states of the $D(\theta_D)$ and $U(\theta_U)$ stripes. With the spontaneous θ -symmetry breaking, a static picture which is formed with the help of the JT cell is shown in Figure 2.

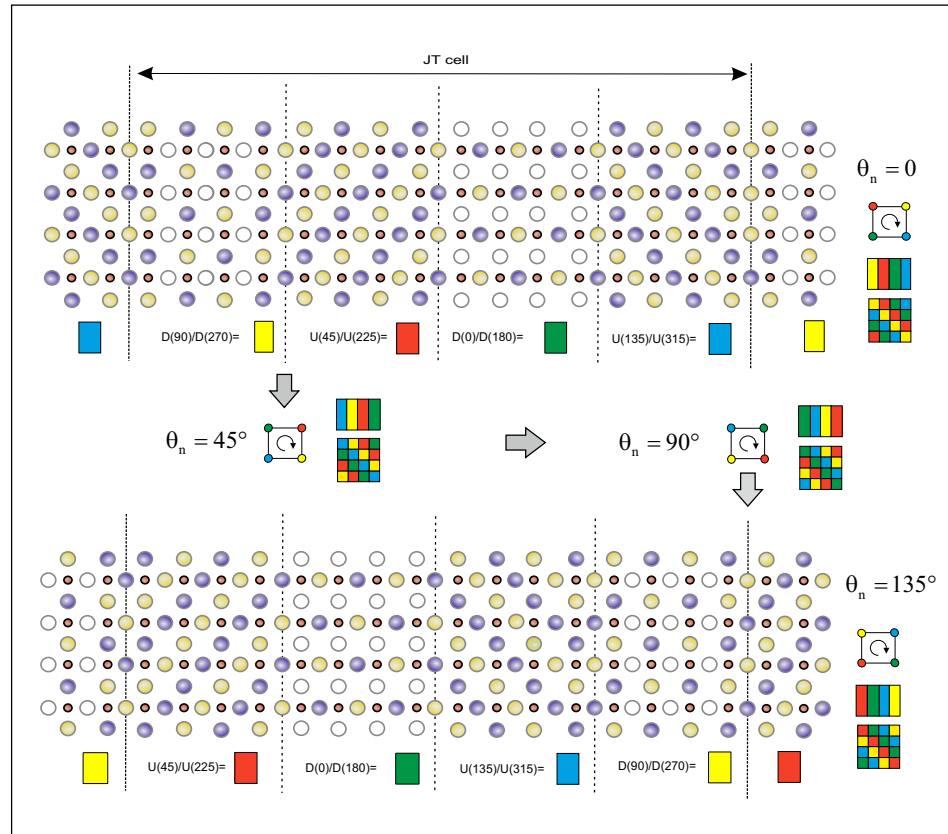


Figure 2. Structural motive for the four-fold degenerate state Ψ_{θ_n} of the novel JT cell. The initial phase $\theta_n, \Psi_{\theta_n}$ —color code and coloring of the graph with $\chi = 2$ are also shown.

Let us consider the JT cell to understand the nature of the inhomogeneous distribution of the hole and spin density in the CuO₂ layer. The cell has the Jahn–Teller (JT) nature, as shown in Figure 3, where the (pseudo) JT effect is non-local and associated with the presence of positively charged LaO rock salt layers. The tilting angle α_U at the orientation angle θ_U corresponds to the relaxation a_{1g} modes, and the tilting angle α_D at the orientation angle θ_D corresponds to the JT active b_{1g} modes.

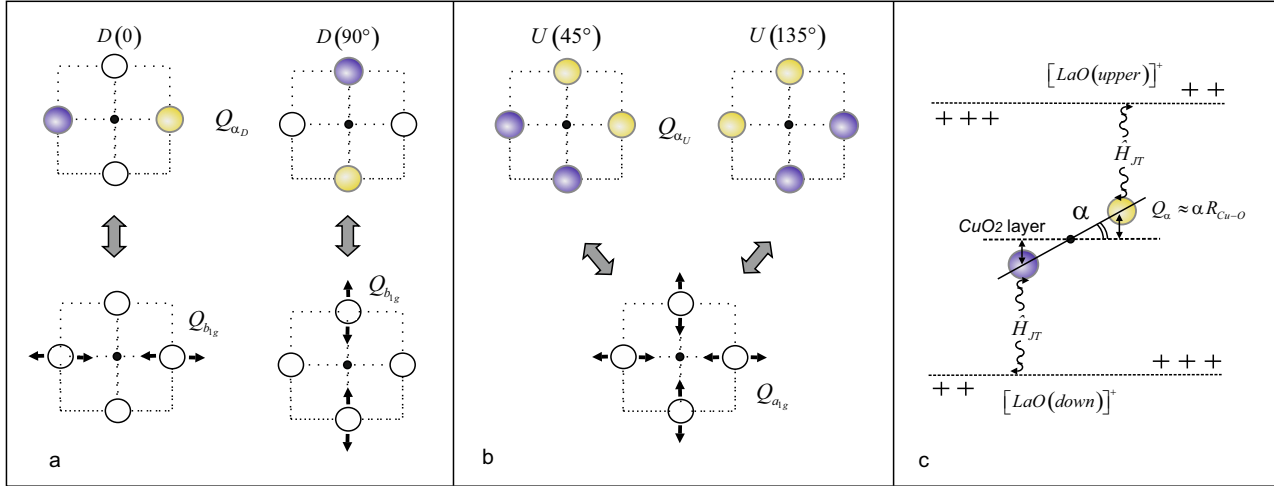


Figure 3. Graphic scheme: (a) b_{1g} tilting modes active in the non-local CuO₆ octahedron JT effect, as well as (b) a_{1g} relaxation modes in the D and U stripes. The arrows in (a,b) show the relationship between the tilting and conventional local modes. (c) Non-local JT effect in the CuO₂ layer surrounded by the symmetrical LaO rock salt layers.

The absence of superconductivity in the AFM CuO layers on graphene [54,55] indicates the key role of rock salt layers in 2D doped cuprates [4]. The direct similarity of the structures of the undoped LCO and non-JT La₂NiO₄ materials [56], where Ni²⁺ ions are in the high spin state $S = 1$, which also indicates the missing JT effect in the $N_0(d^9)$ sector of the configuration space of the CuO₂ layer. However, in the $N_-(d^8)$ sector of the doped LSCO, the hole carriers are in the Zhang–Rice singlet state $^1A_{1g}$ [57], and this is a JT state [58]. Moreover, the JT pseudo-effect depends on the doping concentration in a threshold way. Indeed, the hole carriers in the $D(\theta_D)$ stripes can induce a non-local JT pseudo-effect in the i -th CuO₆ octahedron with a Hamiltonian (see Figure 3).

$$\hat{H}_{JT}^{(i)}(Q_\alpha, Q_\theta) = \varepsilon_{1B_{1g}} \sum_{\sigma} b_{i\sigma}^+ b_{i\sigma} + \varepsilon_{1A_{1g}} \sum_{\sigma} a_{i\sigma}^+ a_{i\sigma} + V_{b_{1g}} Q_\alpha \sum_{\sigma} (a_{i\sigma}^+ b_{i\sigma} + b_{i\sigma}^+ a_{i\sigma}) + U(Q_\alpha, Q_\theta) \quad (1)$$

in the hole sector $N_-(d^8)$ of the configuration space of the CuO₂ layer. Here, $a_{i\sigma}^+ = \eta(\sigma) X_i^{1B_{1g}, \bar{\sigma}b}$ and $b_{i\sigma}^+ = \eta(\sigma) X_i^{1A_{1g}, \bar{\sigma}b}$ are two hole parts of the quasiparticle operator

$$\begin{aligned} d_{i\lambda\sigma}^+ &= X_i^{\sigma b, A_{1g}} + \sum_{h=1A_g, 1B_g} \langle h | d_{i\lambda\sigma}^+ | \sigma_b \rangle X_i^{h, \bar{\sigma}b} \\ &= X_i^{\sigma b, A_{1g}} + \begin{cases} a_{i\sigma}^+, \lambda = 3z^2 - r^2 \\ b_{i\sigma}^+, \lambda = x^2 - y^2 \end{cases} \end{aligned} \quad (2)$$

generating two-hole $^1A_{1g}$ and $^1B_{1g}$ states in the $N_-(d^8)$ sector. If $|h\rangle = |^1A_{1g}\rangle$, then the operator $d_{i\lambda\sigma}^+$ takes the well-known form for the Hubbard model [59]. It is assumed that the $U(Q_\alpha, Q_\theta)$ potential is created by the LaO rock salt layers, and the equilibrium ion positions in the CuO₂ layer can be obtained from the equation $\frac{\partial \hat{H}_{JT}(Q_\alpha, Q_\theta)}{\partial Q_\alpha \partial Q_\theta} = 0$. Here, we use the set θ_D and $\alpha_D \approx 14^\circ \div 18^\circ$, which are observed at $T = 100$ K for the D stripes [50].

The concentration dependence of the magnitude $\alpha_D(x)$ in the JT effect can be obtained using the u/v transformation in the Hamiltonian (1) with the coefficients

$$\begin{aligned} u^2(Q_\alpha) &= \frac{1}{2} \left(1 - \frac{\varepsilon_{1B_{1g}} - \varepsilon_{1A_{1g}}}{D(Q_\alpha)} \right), \\ v^2(Q_\alpha) &= \frac{1}{2} \left(1 + \frac{\varepsilon_{1B_{1g}} - \varepsilon_{1A_{1g}}}{D(Q_\alpha)} \right), \end{aligned} \quad (3)$$

where $D(Q_\alpha) = \sqrt{(\varepsilon_{1B_{1g}} - \varepsilon_{1A_{1g}})^2 + 4(V_{b_{1g}} Q_\alpha)^2}$ and $a_{i\sigma}^+ = v(Q_\alpha)\tilde{a}_{i\sigma}^+ + u(Q_\alpha)\tilde{b}_{i\sigma}^+$, $b_{i\sigma}^+ = v(Q_\alpha)\tilde{b}_{i\sigma}^- - u(Q_\alpha)\tilde{a}_{i\sigma}^+$. Then, the Hamiltonian (1) may be written as

$$\hat{H}_{JT}^{(i)}(Q_\alpha, Q_{\theta_D}) = \varepsilon_-(Q_\alpha) \sum_\sigma \tilde{b}_{i\sigma}^+ \tilde{b}_{i\sigma}^- + \varepsilon_+(Q_\alpha) \sum_\sigma \tilde{a}_{i\sigma}^+ \tilde{a}_{i\sigma}^-, \quad (4)$$

where $\varepsilon_\pm(Q_\alpha) = \frac{1}{2} [\varepsilon_{1A_{1g}} + \varepsilon_{1B_{1g}} \pm D(Q_\alpha)]$ are the energies of the hole quasiparticles in the two-hole singlets $|^1\tilde{A}_{1g}\rangle$ and $|^1\tilde{B}_{1g}\rangle$ taking into account the JT interaction $V_{b_{1g}}$. The equilibrium tilting angle α_D at $U(Q_\alpha, Q_{\theta_D}) \approx (K\alpha^2)/2$ takes the form $\alpha_D(x) = \pm \sqrt{\left(\frac{RV_{b_{1g}}}{K}\right)^2 - \left(\frac{\Delta}{V_{b_{1g}}}\right)^2}$ where $R = \sum_\sigma \langle \tilde{b}_\sigma^+ \tilde{b}_\sigma^- - \tilde{a}_\sigma^+ \tilde{a}_\sigma^- \rangle$. Thus, in the doped LSCO cuprates, there is a hole doping level $x_c = \left\langle X_i^{1\tilde{A}_{1g}} - X_i^{1\tilde{B}_{1g}} \right\rangle = \frac{K\Delta}{V_{b_{1g}}^2}$, and above which, the JT pseudo effect with $\alpha_D \neq 0$ can be observed. At $\Delta = \varepsilon_{1B_{1g}} - \varepsilon_{1A_{1g}} = 0$ [60] we obtain the quadratic hole doping dependence for the JT contribution:

$$\hat{H}_{JT}^{(i)}(Q_{\alpha_D}, Q_{\theta_D}, x) = -E_{JT}^{(0)} R \sum_\sigma (\tilde{b}_{i\sigma}^+ \tilde{b}_{i\sigma}^- - \tilde{a}_{i\sigma}^+ \tilde{a}_{i\sigma}^-), \quad (5)$$

where $E_{JT}^{(0)} = V_{b_{1g}}^2 / 2K$. Any homogeneous hole density at $x < x_c$ will be unstable to the creation of local D areas with a higher hole density $x_D > x_c$ and $\langle \hat{H}_{JT} \rangle = \left\langle \sum_{i=D} \hat{H}_{JT}^{(i)} \right\rangle \neq 0$. The boundaries contribution to the lattice energy is absent, because the boundaries between the stripes are in fact atomically sharp. At the small hole doping, the total JT contribution $\langle \hat{H}_{JT} \rangle \sim x$ due to the increasing width of the D stripes with the constant hole concentration x_D . This is a x_D —constant scenario, where $x_D \geq x_c$.

3. Electron-Hole Pairs in the Superexchange Interaction

Let us consider the superexchange interaction J_{ij} in the static stripe structure in Figure 2. In the case of spontaneous θ -symmetry breaking (the JT cell state Ψ_{θ_i} is non-degenerate), the doped LSCO cuprate has a static nanostructure, where the exchange interaction is missing in the D stripes (where $S_i = 0$), and in the U stripes the superexchange interaction is equal to the one in undoped LCO materials:

$$\hat{H}_S = - \sum_{ij} J_{ij}^{tot} \hat{S}_i \hat{S}_j \quad (6)$$

Here, the interaction $J_{ij}^{tot} = \sum_{h,e} J_{ij}(h, e)$ can be calculated in the adiabatic approximation. Superexchange interaction (6) arises as a result of the superposition of contributions from all possible virtual electron-hole pairs on the interacting i -th and j -th ions (see Figure 4). The sign of the $J_{ij}(h, e)$ contribution to the J_{ij}^{tot} interaction is determined by a simple rule. If the spins of an electron and a hole in a virtual pair are equal, $\hat{S}_h = \hat{S}_e$, this is the AFM contribution. If $\hat{S}_h = \hat{S}_e \pm 1$, it is the FM contribution. Other terms are

missing, and all the electron-hole wave functions $|h\rangle$ and $|e\rangle$ in the hopping integral $t_{ij}^{hn,en} = \sum_{\lambda\lambda'} t_{ij}(\lambda\lambda') \sum_{\sigma} \gamma_{\lambda\sigma}^*(hn) \gamma_{\lambda'\sigma}(en)$ [61–63] in the superexchange

$$J_{ij}^{tot} = \sum_{h,e} J_{ij}(hn,en), J_{ij}(hn,en) = \frac{2(t_{ij}^{hn,en})^2}{\Delta(hn,en)}, \quad (7)$$

$$\Delta(hn,en) = \varepsilon_h + \varepsilon_e - 2\varepsilon_n$$

are calculated in the adiabatic approximation, where

$$\begin{aligned} \gamma_{i\lambda\sigma}(hn) &= \langle h | d_{i\lambda\sigma}^+ | n \rangle = \langle (N_-, S_h) | d_{i\lambda\sigma}^+ | (N_0, S_n) \rangle \\ \gamma_{i\lambda\sigma}(en) &= \langle e | d_{i\lambda\sigma} | n \rangle = \langle (N_+, S_e) | d_{i\lambda\sigma} | (N_0, S_n) \rangle \end{aligned} \quad (8)$$

The pairs of indices hn and en run over all possible quasiparticle excitations (e, n) and (h, n) between many-electron states $|n\rangle$ and $|e(h)\rangle$ with the energies ε_n and $\varepsilon_{e(h)}$ in the sectors N_0 and N_{\pm} of the configuration space in Figure 4.

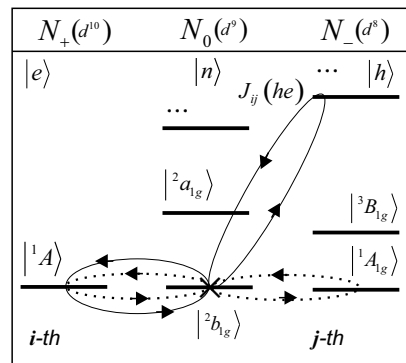


Figure 4. Graphic representation of the electron-hole pairs for the interacting i -th and j -th Cu^{2+} ions. Each pair corresponds to a double exchange loop (solid or dotted lines).

These quasiparticle excitations are described by non-diagonal elements $t_{ij}^{nh,ne}$. In the Hubbard's model there is only one such element corresponding to the excitations between lower and upper Hubbard bands. In cuprates, the main contribution from the electron-hole pair with $|n\rangle = {}^2b_{1g}$, $|h\rangle = {}^1A_{1g}$ and $|e\rangle = {}^1A$ has the AFM character $J_{ij}^{tot} \approx J_{ij}^{(U)} ({}^1A^2b_{1g}, {}^1A_{1g}^2b_{1g})$ (see Figure 4) [64], where

$$J_{ij}^{(U)} ({}^1A^2b_{1g}, {}^1A_{1g}^2b_{1g}) = \frac{2t_{ij}^2}{\Delta({}^1A^2b_{1g}, {}^1A_{1g}^2b_{1g})} \approx 0.15 \text{ eV} \quad (9)$$

where $\Delta({}^1A^2b_{1g}, {}^1A_{1g}^2b_{1g}) = \varepsilon_{1A_{1g}} - 2(\varepsilon_{2b_{1g}} - V_{a_{1g}} \alpha_U) = U_H$ and $\varepsilon_{1A_{1g}} = 2(\varepsilon_{2b_{1g}} - V_{a_{1g}} \alpha_U) + U_H$. However, the transverse percolation of the exchange interaction $J_{i_R j_B}^{tot}$, where i_R and j_B in the octahedra CuO_6 are in different red(R) and blue(B) stripes in the static regular Y/R/G/B... stripe structure, is unlikely.

If there is no spontaneous θ -symmetry breaking and the JT cell state is four-fold degenerate, then the exchange interaction in the JT cell presented above is incomplete, due to the the novel configuration space. Here, the i -th CuO_6 octahedron (the black point in Figure 5) can simultaneously be in the U and D stripe states of any color of the four possible R, B and G, Y. In addition to the initial quasiparticles in the static stripe structure, specific hole quasiparticles appear in the CuO_2 layer, but they are accompanied by changes $\delta\alpha = \alpha_D - \alpha_U$ and $\delta\theta = \theta_D - \theta_U$ shown in Figure 5.

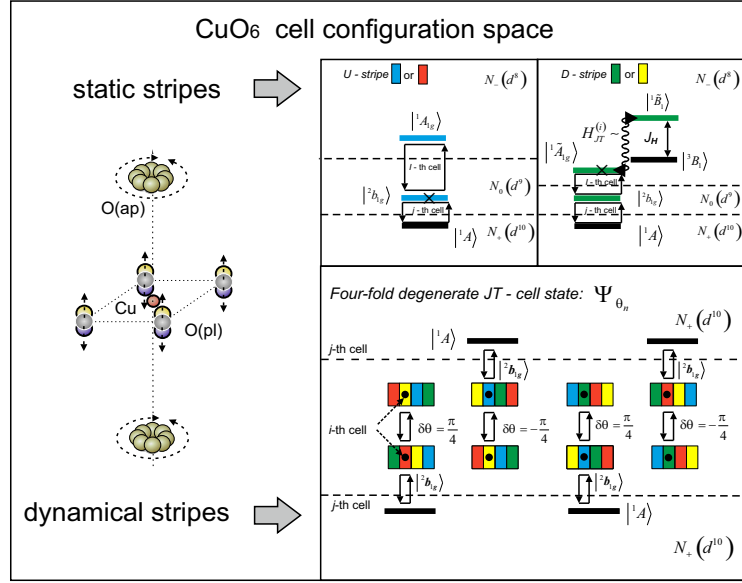


Figure 5. Left graphical representation shows the anisotropic non-local effects in the CuO₆ octahedron located in the JT cell with the fourfold degeneracy. The right diagram presents the electron-hole pairs contributing to the exchange interaction when both the *i*-th and *j*-th magnetic ions are in the JT cell. Here, the *U* and *D* stripe widths are the same to demonstrate the appearance of an ideal CuO₂ layer with mobile hole carriers only with the equal stripe widths.

To obtain contributions into $J_{ij}(hn, en)$ from the electron-hole pairs with a change in the angles $\delta\alpha$ and $\delta\theta = \pm 45^\circ$ in the JT cell, we need the *i*-th CuO₆ octahedron $|h_{\theta_D\alpha_D}\rangle$ and $|n_{\theta_U\alpha_U}\rangle$ states, where the indices *U* and *D* denote the stripe affiliation for the *i*-th octahedron

$$|h_{\theta_D\alpha_D}\rangle = |\tilde{h}\rangle|\chi_{\theta_D}\chi_{\alpha_D}\rangle; |n_{\theta_U\alpha_U}\rangle = |n\rangle|\chi_{\theta_U}\chi_{\alpha_U}\rangle, \quad (10)$$

where $|\tilde{h}\rangle = |^1\tilde{A}_{1g}\rangle, |^1\tilde{B}_{1g}\rangle$ and $|n\rangle = |^2b_{1g}\rangle$. Each of the *R, G, B, Y* colors in Figure 2 corresponds to a harmonic oscillator wave function $|\chi_\theta\rangle$ with a displaced 2D oscillator. These states differ by $|\chi_{\alpha_D}(Q_\alpha + \alpha_D)\rangle, |\chi_{\theta_D}(Q_{\theta_D})\rangle$ and $|\chi_{\alpha_U}(Q_\alpha + \alpha_U)\rangle, |\chi_{\theta_U}(Q_{\theta_U})\rangle$, and the matrix elements $\gamma_{\lambda\sigma}(r)$ in Equation (8) for the *i*-th CuO₆ octahedron cell will be calculated with the functions $|h_{\theta_D\alpha_D}\rangle$ and $|n_{\theta_U\alpha_U}\rangle$ located at the four equivalent nuclear configurations of the JT cell corresponding to the phase θ_n (see black dot in Figure 5). The matrix elements $\gamma_{\lambda\sigma}(hn)$ contain vibronic reduction factors or partial dynamic quenching [65]:

$$J_{ij}(^1\tilde{A}_{1g}, ^1A) = \frac{2\left(t_{ij}^{^1\tilde{A}_{1g}^2b_{1g}, ^1A^2b_{1g}}\right)^2}{\Delta(^1\tilde{A}_{1g}^2b_{1g}, ^1A^2b_{1g})} \approx \frac{2v^2(\alpha_D) \cdot t_{ij}^2(x^2, x^2)}{\Delta(^1\tilde{A}_{1g}^2b_{1g}, ^1A^2b_{1g})} \cdot \exp\left\{-v\frac{\delta\theta^2 + \delta\alpha^2}{2}\right\}, \quad (11)$$

where $v = K/\hbar\omega_D$ (ω_D —Debye frequency) and

$$t_{ij}^{^1\tilde{A}_{1g}^2b_{1g}, ^1A^2b_{1g}} \approx t_{ij}(x^2, x^2)v(\alpha_D) \sum_{\sigma} \gamma_{x^2\sigma}^*(^1A_{1g}, ^2b_{1g}) \gamma_{x^2\sigma}(^1A, ^2b_{1g}) \cdot \langle\chi_{i\theta_D}|\chi_{i\theta_U}\rangle \langle\chi_{i\phi_D}|\chi_{i\phi_U}\rangle, \quad (12)$$

where $\Delta(^1\tilde{A}_{1g}^2b_{1g}, ^1A^2b_{1g}) = 2[\varepsilon_-(\alpha_D) - \varepsilon_{2b_{1g}}] + U_H, t_{ij}(x^2, x^2) \gg t_{ij}(z^2, z^2)$, and

$$\begin{aligned} &\langle\chi_{i\theta_D}|\chi_{i\theta_U}\rangle \cdot \langle\chi_{i\alpha_D}|\chi_{i\alpha_U}\rangle = \\ &\langle\chi_{i\alpha_D}(Q_\alpha + \alpha_D)\chi_{i\theta_D}(\theta_D)|\chi_{i\alpha_U}(Q_\alpha + \alpha_U)\chi_{i\theta_U}(\theta_U)\rangle \\ &\approx \exp\left\{-v(\delta\theta^2 + \delta\alpha^2)/4\right\} \end{aligned} \quad (13)$$

with $\delta\alpha = \alpha_D - \alpha_U \approx 9^\circ \div 13^\circ$. With the absence of spontaneous θ -symmetry breaking, the homogeneous superexchange interaction in the hole-doped LSCO cuprates is equal to

$$J_{ij}^{tot} \approx J_{ij} \left({}^1\tilde{A}_{1g} {}^2b_{1g}, {}^1A_1 {}^2b_{1g} \right) \cdot v^2(\alpha_D) \cdot \exp \left\{ -v \frac{\delta\theta^2 + \delta\alpha^2}{2} \right\}. \quad (14)$$

This result (14) is independent of the choice of the i and j pair of the interacting CuO_6 octahedra and the exchange J_{ij}^{tot} is homogeneous in the ideal CuO_2 layer with nonlocal effects. Indeed, the neutron experiments in LCO cuprates demonstrate the thermal anisotropic motion [66] similar to the oxygen ion motion shown in Figure 5. Similar reduction factors in n doped LNCO cuprates are impossible, since there is no JT effect in the N_+ (d^{10}) electron sector.

4. Discussion and Conclusions

The JT pseudo effect in the N_- (d^8) hole sector with the hole concentration x in the range $0 < x < x_c$ is accompanied by the charge and spin inhomogeneities due to the nonzero tilting angle $\alpha_D \approx 14 \div 18^\circ$ [50] of the CuO_6 octahedra at the orientation angle $\theta_D = 0^\circ, 90^\circ, 180^\circ, 270^\circ$ in the $D(\theta_D)$ stripes (see Figure 1). The $U(\theta_U)$ stripes with the CuO_6 octahedra tilted at an angle $\alpha_U \approx 5^\circ$ [67] and oriented at an angle $\theta_U = 45^\circ, 135^\circ, 225^\circ, 315^\circ$ form dielectric regions. The observed regular line and checkerboard stripe structures [68,69] with the chromatic number $\chi = 2$ generate a novel element of symmetry in the CuO_2 layer: simultaneously rotating all the tilted CuO_6 octahedra by the angle $\delta\theta_n = n \cdot (45^\circ)$ (where $n = 1 \div 4$) around the c axis. We can choose a novel JT cell, the initial structure and number of hole carriers and spins in the JT cell will be retained during its translation. The state Ψ_{θ_n} of the JT cell is fourfold degenerate by the initial phase $\theta_n = 0, 45^\circ, 90^\circ, 135^\circ$ (see Figure 2). In particular, any CuO_6 octahedron can be located simultaneously, both in the $U(\theta_U)$ and $D(\theta_D)$ stripes without any well-specified orientation $\theta_D(\theta_U)$ and tilting $\alpha_D(\alpha_U)$ angles. The exchange interaction J_{ij}^{tot} will be different, depending on whether the spontaneous phase θ -symmetry breaking occurs or not:

- (i) The spontaneous θ -symmetry breaking leads to a static spatial distribution of the $U(\theta_U)$ and $D(\theta_D)$ stripes in the doped LSCO. The static distribution originates from the different stripe width and shape, when there is no θ_n phase degeneracy. The signature of the static structure *does not* depend on the experimental timescale ranging from 10^{-6} s to 10^{-15} s, but is sensitive to the temperature and hole concentration [47]. In the static structure of the CuO_2 layer, the superexchange interaction has the Anderson's form $J_{ij}^{(U)} = 2t^2/U_H$ for the interacting ions Cu^{2+} with spin 1/2, but is limited in space by the $U(\theta_U)$ stripes with the zero hole concentration.
- (ii) Without spontaneous θ -symmetry breaking a novel JT cell can be constructed in the periodic stripe nanostructure with the fourfold degenerate Ψ_{θ_n} state. The ideal CuO_2 structure with nonlocal anisotropic effects and the homogeneous superexchange are restored. The stripe boundaries, spin and charge inhomogeneities disappear, and the superexchange is suppressed from its magnitude $J_{ij}^{(U)}$ (in the undoped LCO cuprate) by the exponential factor $J_{ij}^{tot} \approx J_{ij}^{(U)} \cdot v^2(\alpha_D) \cdot \exp \{ -v(\delta\alpha_D^2 + \delta\theta_D^2)/2 \}$ due to dynamic quenching for the CuO_6 octahedra. We can evaluate the E_{JT} magnitude as $E_{JT} \approx \hbar\omega_D$, where $E_{JT} = K(\delta\alpha^2 + \delta\theta^2)$, because the stripe fluctuations are observed at the temperature ~ 100 K. Thus $J_{ij}^{tot} \approx 0.61 \cdot J_{ij}^U \cdot v^2(\alpha_D)$, where $0.5 \leq v^2(\alpha_D) \leq 1$ and $J_{ij}^U \approx 0.15$ eV. The stripe signatures noticeably weaken with the decreasing temperature, but they are still detected as density waves of the hole pairs [43–46].

There is no direct analogy with a free rotator, since there is no continuous series θ_D of the tilted CuO_6 octahedra for which the potential energy is minimal. Only tunneling and hopping effects are possible at the low and high temperatures, respectively. This conclusion does not contradict the results, where the low-temperature optical pump, soft X-ray probe

measurements [13] detected the unexpected gapless nature of the charge ordering. Indeed, the characteristic tunneling JT splitting $\leq 10 \text{ meV}$ [70] has the energy scale of the transverse fluctuations observed in LBCO [13], and the magneto-optical measurements identify the effects of time reversal symmetry breaking [71–74].

Note that a period of the charge stripes sequence $U/D/U/\dots$ is two times less than the period of the lattice stripe structure $Y/R/G/B\dots$, since the hole concentration x_D does not depend on the orientation angle θ_D . In (nonpseudo) Jahn–Teller materials, where $x_c = 0$ such as 3D AMeO₃ perovskites with regular MeO₆ octahedra, the hole segregation into strip structures is impossible. The hole concentration x_D in the D stripes does not depend on the total hole concentration x in the CuO₂ layer, but the total D stripe area rises with increasing hole doping. This x_D constant scenario has clear experimental features such as Fermi level pinning, where a shift of chemical potential is suppressed in the underdoped region of p type LSCO cuprates [75]. In the n type LNCO cuprates, the JT effect in N_+ (d^{10}) configuration sector is missing. In contrast to LSCO, the superexchange interaction J_{ij} should not be subject to dynamic quenching, and the monotonous increase of the chemical potential is consistent with the absence of stripe fluctuations [75]. The dynamic quenching magnitude in Equation (14) decreases exponentially with the increasing Debye temperature $\hbar\omega_D/k_B$. A similar trend for the critical temperature T_C in the La, Y, Tl and Hg based cuprates with Debye temperatures from 200 K to 600 K was found in Refs. [76,77]. Note also that our arguments in favor of the JT nature of the charge inhomogeneity is an alternative to the fact that the competition between the kinetic energy and Coulomb repulsion could cause holes to segregate into strip structures [78].

Author Contributions: Conceptualization, V.A.G.; investigation, V.A.G. and S.I.P.; writing—review and editing, V.A.G. and S.I.P.; supervision, V.A.G. All authors have read and agreed to the published version of the manuscript.

Funding: This work was supported by the Russian Science Foundation, research grant RSF No.22-22-00298.

Data Availability Statement: We are grateful to the colleagues who made useful comments after the draft paper in arXiv:2205.11959 [cond-mat.str-el].

Conflicts of Interest: The authors declare no conflict of interest.

References

1. Bussmann-Holder, A.; Keller, H.; Bianconi, A. (Eds.) *High-T_C Copper Oxide Superconductors and Related Novel Materials*; Springer Series in Materials Science; Springer International Publishing AG: Berlin/Heidelberg, Germany, 2017; Volume 255.
2. Egami, T. Alex and the Origin of High-Temperature Superconductivity. In *High-T_C Copper Oxide Superconductors and Related Novel Materials*; Springer Series in Materials Science; Springer International Publishing AG: Berlin/Heidelberg, Germany, 2017; pp. 35–46.
3. Benedek, G.; Muller, K. *Phase Separation in Cuprate Superconductors*; World Scientific: Singapore, 1993.
4. Bianconi, A.; Agrestini, S.; Bianconi, G.; Di Castro, D.; Saini, N. A Quantum Phase Transition Driven by the Electron Lattice Interaction Gives High T_C Superconductivity. *J. Alloys Compd.* **2001**, *317*, 537–541. [[CrossRef](#)]
5. Zhao, H.; Ren, Z.; Rachmilowitz, B.; Schneeloch, J.; Zhong, R.; Gu, G.; Wang, Z.; Zeljkovic, I. Charge stripe crystal phase in an insulating cuprate. *Nat. Mater.* **2019**, *18*, 103–107. [[CrossRef](#)] [[PubMed](#)]
6. Maggio-Aprile, I.; Berthod, C.; Jenkins, N.; Fasano, Y.; Piriou, A.; Fischer, O. *Nanoscience and Engineering in Superconductivity. NanoScience and Technolog*; Chapter Scanning Tunneling Spectroscopy of High T_C Cuprates; Springer: Berlin/Heidelberg, Germany, 2010.
7. Fischer, O.; Kugler, M.; Maggio-Aprile, I.; Berthod, C.; Renner, C. Scanning tunneling spectroscopy of high-temperature superconductors. *Rev. Mod. Phys.* **2007**, *79*, 353–419. [[CrossRef](#)]
8. da Silva Neto, E.; Aynajian, P.; Frano, A.; Comin, R.; Schierle, E.; Weschke, E.; Gyenis, A.; Wen, J.; Schneeloch, J.; Xu, Z.; et al. Ubiquitous Interplay Between Charge Ordering and High-Temperature Superconductivity in Cuprates. *Science* **2014**, *343*, 393–396. [[CrossRef](#)] [[PubMed](#)]
9. Ma, J. Scanning Tunneling Microscopy Studies of Single Layer High-T_C Cuprate Bi₂Sr_{2-x}La_xCuO_{6+δ}. Ph.D. Thesis, Boston College, Chestnut Hill, MA, USA, 2009.
10. Lanzara, A.; Saini, N.; Brunelli, M.; Valletta, A.; Bianconi, A. Evidence for onset of charge density wave in the La-based Perovskite superconductors. *J. Supercond.* **1997**, *10*, 319–321. [[CrossRef](#)]

11. Campi, G.; Bianconi, A.; Poccia, N.; Bianconi, G.; Barba, L.; Gand, A.; Innocenti, D.; Karpinski, J.; Zhigadlo, N.; Kazakov, S.; et al. Inhomogeneity of charge-density-wave order and quenched disorder in a high-Tc superconductor. *Nature* **2015**, *525*, 359–362. [[CrossRef](#)]
12. Comin, R.; Damascelli, A. Resonant X-ray Scattering Studies of Charge Order in Cuprates. *Annu. Rev. Condens. Matter Phys.* **2016**, *7*, 369–405. [[CrossRef](#)]
13. Mitrano, M.; Lee, S.; Husain, A.; Delacretaz, L.; Zhu, M.; de la Pena Munoz, G.; Sun, S.X.-L.; Joe, Y.I.L.; Reid, A.; Wandel, S.; et al. Ultrafast time-resolved X-ray scattering reveals diffusive charge order dynamics in $\text{La}_{2-x}\text{Ba}_x\text{CuO}_4$. *Sci. Adv.* **2019**, *5*, eaax3346. [[CrossRef](#)]
14. Campi, G.; Bianconi, A. Functional Nanoscale Phase Separation and Intertwined Order in Quantum Complex Materials. *Condens. Matter* **2021**, *6*, 40. [[CrossRef](#)]
15. Zaanen, J.; Gunnarsson, O. Charged magnetic domain lines and the magnetism of high-Tc oxides. *Phys. Rev. B* **1989**, *40*, 7391–7394. [[CrossRef](#)]
16. Machida, K. Magnetism in La_2CuO_4 based compounds. *Phys. C* **1989**, *158*, 192–196. [[CrossRef](#)]
17. Tranquada, J.M.; Sternlieb, B.J.; Axe, J.D.; Nakamura, Y.; Uchida, S. Evidence for stripe correlations of spins and holes in copper oxide superconductors. *Nature* **1995**, *375*, 561–563. [[CrossRef](#)]
18. Fujita, M.; Goka, H.; Yamada, K.; Tranquada, J.M.; Regnault, L.P. Stripe order, depinning, and fluctuations in $\text{La}_{1.875}\text{Ba}_{0.125}\text{CuO}_4$ and $\text{La}_{1.875}\text{Ba}_{0.075}\text{Sr}_{0.050}\text{CuO}_4$. *Phys. Rev. B* **2004**, *70*, 104517. [[CrossRef](#)]
19. Hucker, M.; van Zimmermann, M.; Gu, G.D.; Xu, Z.J.; Wen, J.S.; Xu, G.; Kang, H.J.; Zheludev, A.; Tranquada, J.M. Stripe order in superconducting $\text{La}_{2-x}\text{Ba}_x\text{CuO}_4$ ($0.095 < x < 0.155$). *Phys. Rev. B* **2011**, *83*, 104506.
20. Fujita, M.; Hiraka, H.; Matsuda, M.; Matsuura, M.; Tranquada, J.; Wakimoto, S.; Xu, G.; Yamada, K. Progress in Neutron Scattering Studies of Spin Excitations in High-Tc Cuprates. *J. Phys. Soc. Jpn.* **2012**, *81*, 011007–011025. [[CrossRef](#)]
21. Wen, J.J.; Huang, H.; Lee, S.J.; Jang, H.; Knight, J.; Lee, Y.S.; Fujita, M.; Suzuki, K.M.; Asano, S.; Kivelson, S.A.; et al. Observation of two types of charge-density-wave orders in superconducting $\text{La}_{2-x}\text{Sr}_x\text{CuO}_4$. *Nat. Commun.* **2019**, *10*, 3269. [[CrossRef](#)]
22. Miao, H.; Fabbri, G.; Koch, R.J.; Mazzone, D.G.; Nelson, C.S.; Acevedo-Esteves, R.; Gu, G.D.; Li, Y.; Yilmaz, T.; Kaznatcheev, K.; et al. Charge density waves in cuprate superconductors beyond the critical doping. *NPJ Quantum Mater.* **2021**, *6*, 31. [[CrossRef](#)]
23. Ma, Q.; Rule, K.C.; Cronkwright, Z.W.; Dragomir, M.; Mitchell, G.; Smith, E.M.; Chi, S.; Kolesnikov, A.I.; Stone, M.B.; Gaulin, B.D. Parallel spin stripes and their coexistence with superconducting ground states at optimal and high doping in $\text{La}_{1.6-x}\text{Nd}_{0.4}\text{Sr}_x\text{CuO}_4$. *Phys. Rev. Res.* **2021**, *3*, 023151. [[CrossRef](#)]
24. Anderson, P.W. The Resonating Valence Bond State in La_2CuO_4 and Superconductivity. *Science* **1987**, *235*, 1196–1198. [[CrossRef](#)]
25. Scalapino, D. The Case for $d_{x^2-y^2}$ Pairing in the Cuprate Superconductors. *Phys. Rep.* **1995**, *250*, 329–365. [[CrossRef](#)]
26. Dagotto, E. Correlated Electrons in High-Temperature Superconductors. *Rev. Mod. Phys.* **1994**, *66*, 763–841. [[CrossRef](#)]
27. Izyumov, Y.A. Spin-fluctuation mechanism of high-Tc superconductivity and order-parameter symmetry. *Physics-Uspeski* **1999**, *42*, 215–243. [[CrossRef](#)]
28. Anderson, P.W. New Approach to the Theory of Superexchange Interactions. *Phys. Rev.* **1959**, *115*, 2–13. [[CrossRef](#)]
29. Coldea, R.; Hayden, S.M.; Aeppli, G.; Perring, T.; Frost, C.D.; Mason, T.E.; Cheong, S.W.; Fisk, Z. Spin Waves and Electronic Interactions in La_2CuO_4 . *Phys. Rev. Lett.* **2001**, *86*, 5377–5380. [[CrossRef](#)] [[PubMed](#)]
30. Bascaran, G.; Zou, Z.; Anderson, P.W. The resonating valence bond state and high-Tc superconductivity—A mean field theory. *Solid State Commun.* **1987**, *63*, 973–976. [[CrossRef](#)]
31. Gros, C.; Joynt, R.; Rice, T.M. Antiferromagnetic correlations in almost-localized Fermi liquids. *Phys. Rev. B* **1987**, *36*, 381–393. [[CrossRef](#)] [[PubMed](#)]
32. Kotliar, G.; Liu, J. Superexchange mechanism and d-wave superconductivity. *Phys. Rev. B* **1988**, *38*, 5142–5145. [[CrossRef](#)]
33. Suzumura, Y.; Hasegawa, Y.; Fukuyama, H. Mean Field Theory of RVB and Superconductivity. *J. Phys. Soc. Jpn.* **1988**, *57*, 2768–2778. [[CrossRef](#)]
34. Prelovsek, P.; Ramsak, A. Spin-fluctuation mechanism of superconductivity in cuprates. *Phys. Rev. B* **2005**, *72*, 012510. [[CrossRef](#)]
35. Plakida, N.M.; Anton, L.; Adam, S.; Adam, G. Exchange and Spin-Fluctuation Mechanisms of Superconductivity in Cuprates. *J. Exp. Theor. Phys.* **2003**, *97*, 331–342. [[CrossRef](#)]
36. Rossat-Mignod, J.; Regnault, L.P.; Vettier, C.; Bourges, P.; Burlet, P.; Bossy, J.; Henry, J.Y.; Lapertot, G. Neutron scattering study of the $\text{YBa}_2\text{Cu}_3\text{O}_{6+x}$ system. *Phys. C Supercond.* **1991**, *185–189*, 86–92. [[CrossRef](#)]
37. Fong, H.F.; Bourges, P.; Sidis, Y.; Regnault, L.P.; Bossy, J.; Ivanov, A.; Milius, D.L.; Aksay, I.A.; Keimer, B. Spin susceptibility in underdoped $\text{YBa}_2\text{Cu}_3\text{O}_{6+x}$. *Phys. Rev. B* **2000**, *61*, 14773–14776. [[CrossRef](#)]
38. Dai, P.; Mook, H.A.; Hunt, R.D.; Dogan, F. Evolution of the resonance and incommensurate spin fluctuations in superconducting $\text{YBa}_2\text{Cu}_3\text{O}_{6+x}$. *Phys. Rev. B* **2001**, *63*, 054525. [[CrossRef](#)]
39. Scalapino, D.J. A common thread: The pairing interaction for unconventional superconductors. *Rev. Mod. Phys.* **2012**, *84*, 1383. [[CrossRef](#)]
40. Vasala, S.; Cheng, J.G.; Yamauchi, H.; Goodenough, J.B.; Karppinen, M. Synthesis and Characterization of $\text{Sr}_2\text{Cu}(\text{W}_{1-x}\text{Mo}_x)\text{O}_6$: A Quasi-Two-Dimensional Magnetic System. *Chem. Mater.* **2012**, *24*, 2764–2774. [[CrossRef](#)]
41. Katukuri, V.M.; Babkevich, P.; Mustonen, O.; Walker, H.C.; Fak, B.; Vasala, S.; Karppinen, M.; Ronnow, H.M.; Yazyev, V.O. Exchange Interactions Mediated by Nonmagnetic Cations in Double Perovskites. *Phys. Rev. Lett.* **2020**, *124*, 077202. [[CrossRef](#)]

42. Thakur, G.S.; Feng, H.L.; Schnelle, W.; Felser, C.; Jansen, M. Structure and magnetism of new A- and B-site ordered double perovskites $\text{ALaCuO}_5\text{O}_6$ (A = Ba and Sr). *J. Solid State Chem.* **2021**, *293*, 121784. [[CrossRef](#)]
43. Li, Y.; Terzic, J.; Baity, P.G.; Popovic, D.; Gu, G.D.; Li, Q.; Tsvelik, A.M.; Tranquada, J.M. Tuning from failed superconductor to failed insulator with magnetic field. *Sci. Adv.* **2019**, *5*, eaav7686. [[CrossRef](#)]
44. Du, Z.; Li, H.; Joo, S.H.; Donoway, E.P.; Lee, J.; Seamus Davis, J.C.; Gu, G.; Johnson, P.D.; Fujita, K. Imaging the energy gap modulations of the cuprate pair-density-wave state. *Nature* **2020**, *580*, 65–70. [[CrossRef](#)]
45. Tsvelik, A.M. Superconductor-metal transition in odd-frequency-paired superconductor in a magnetic field. *Proc. Natl. Acad. Sci. USA* **2019**, *116*, 12729–12732. [[CrossRef](#)]
46. Chen, W.; Ren, W.; Kennedy, N.; Hamidian, M.H.; Uchida, S.; Eisaki, H.; Johnson, P.D.; O'Mahony, S.M.; Seamus Davis, J.C. Identification of a nematic pair density wave state in $\text{Bi}_2\text{Sr}_2\text{CaCu}_2\text{O}_{8+x}$. *Proc. Natl. Acad. Sci. USA* **2022**, *119*, e2206481119. [[CrossRef](#)] [[PubMed](#)]
47. Lanzara, A.; Zhao, G.M.; Saini, N.L.; Bianconi, A.; Conder, K.; Keller, H.; Muller, K.A. Oxygen-isotope shift of the charge-stripe ordering temperature in $\text{La}_{2-x}\text{Sr}_x\text{CuO}_4$ from X-ray absorption spectroscopy. *J. Phys. Condens. Matter* **1999**, *11*, L541–L546. [[CrossRef](#)]
48. Rubio, D.; Mesot, J.; Conder, K.; Janssen, S.; Mutka, H.; Furrer, A.J. Doping and isotope dependence of the pseudogap in high- T_c cuprates observed by neutron crystal-field spectroscopy: A fast local probe. *J. Supercond.* **2000**, *13*, 727–730. [[CrossRef](#)]
49. Suryadijaya, T.; Sasagawa, T.; Takagi, H. Oxygen isotope effect on charge/spin stripes in $\text{La}_{1.8-x}\text{Eu}_{0.2}\text{Sr}_x\text{CuO}_4$. *Phys. C Supercond.* **2005**, *426–431*, 402–406. [[CrossRef](#)]
50. Bianconi, A.; Saini, N.L.; Lanzara, A.; Missori, M.; Rossetti, T.; Oyanagi, H.; Yamaguchi, H.; Oka, K.; Ito, T. Determination of the Local Lattice Distortions in the CuO_2 Plane of $\text{La}_{1.85}\text{Sr}_{0.15}\text{CuO}_4$. *Phys. Rev. Lett.* **1996**, *76*, 3412–3415. [[CrossRef](#)] [[PubMed](#)]
51. Gavrichkov, V.A.; Shan'ko, Y.; Zamkova, N.G.; Bianconi, A. Is There Any Hidden Symmetry in the Stripe Structure of Perovskite High-Temperature Superconductors? *J. Phys. Chem. Lett.* **2019**, *10*, 1840–1844. [[CrossRef](#)]
52. Glazer, A.M. A Brief History of Tilts. *Phase Transit.* **2011**, *84*, 405–420. [[CrossRef](#)]
53. Woodward, R.B.; Hoffmann, R. *The Conservation of Orbital Symmetry*; Verlag Chemie GmbH; Academic Press Inc.: Cambridge, MA, USA, 1971.
54. Kano, E.; Kvashnin, D.G.; Sakai, S.; Chernozatonskii, L.A.; Sorokin, P.B.; Hashimoto, A.; Takeguchi, M. One-atom-thick 2D copper oxide clusters on graphene. *Nanoscale* **2017**, *9*, 3980–3985. [[CrossRef](#)]
55. Kvashnin, D.G.; Kvashnin, A.G.; Kano, E.; Hashimoto, A.; Takeguchi, M.; Naramoto, H.; Sakai, S.; Sorokin, P.B. Two-Dimensional CuO Inside the Supportive Bilayer Graphene Matrix. *J. Phys. Chem. C* **2019**, *123*, 17459–17465. [[CrossRef](#)]
56. Rodriguez-Carvajal, J.; Fernandez-Diaz, M.T.; Martinez, J.L. Neutron diffraction study on structural and magnetic properties of La_2NiO_4 . *J. Phys. Condens. Matter* **1991**, *3*, 3215–3234. [[CrossRef](#)]
57. Zhang, F.C.; Rice, T.M. Effective Hamiltonian for the superconducting Cu oxides. *Phys. Rev. B* **1988**, *37*, 3759–3761. [[CrossRef](#)] [[PubMed](#)]
58. Bersuker, G.I.; Gorinchoy, N.N.; Polinger, V.Z.; Solonenko, A.O. Jahn-Teller Mechanism of Coupling in the HTSC. *Supercond. Phys. Chem. Eng.* **1992**, *5*, 1003–1013.
59. Hubbard, J. Electron correlations in narrow bands. *Proc. Roy. Soc.* **1964**, *84*, 455–560. [[CrossRef](#)]
60. Gavrichkov, V.A.; Gavrichkov, S.A. The Jahn-Teller instability criterion for resonance impurity states. *Phys. Lett. A* **1990**, *145*, 353–357. [[CrossRef](#)]
61. Gavrichkov, V.A.; Polukeev, S.I.; Ovchinnikov, S.G. Cation spin and superexchange interaction in oxide materials below and above spin crossover under high pressure. *Phys. Rev. B* **2020**, *101*, 094409. [[CrossRef](#)]
62. Gavrichkov, V.A.; Polukeev, S.I.; Ovchinnikov, S.G. Contribution from optically excited many-electron states to the superexchange interaction in Mott-Hubbard insulators. *Phys. Rev. B* **2017**, *95*, 144424. [[CrossRef](#)]
63. Mikhaylovskiy, R.; Huisman, T.; Gavrichkov, V.; Polukeev, S.I.; Ovchinnikov, S.; Afanasiev, D.; Pisarev, R.; Rasing, T.; Kimel, A. Resonant Pumping of d-d Crystal Field Electronic Transitions as a Mechanism of Ultrafast Optical Control of the Exchange Interactions in Iron Oxides. *Phys. Rev. Lett.* **2020**, *125*, 157201. [[CrossRef](#)]
64. Gavrichkov, V.A.; Pchelkina, Z.V.; Nekrasov, I.A.; Ovchinnikov, S.G. Pressure effect on the energy structure and superexchange interaction in undoped orthorhombic La_2CuO_4 . *Int. J. Mod. Phys. B* **2016**, *30*, 1650180. [[CrossRef](#)]
65. Ham, F.S. Dynamical Jahn-Teller Effect in Paramagnetic Resonance Spectra: Orbital Reduction Factors and Partial Quenching of Spin-Orbit Interaction. *Phys. Rev.* **1965**, *138*, A1727–A1740. [[CrossRef](#)]
66. Hafliger, P.S.; Gerber, S.; Pramod, R.; Schnells, V.I.; dalla Piazza, B.; Chati, R.; Pomjakushin, V.; Conder, K. Quantum and thermal ionic motion, oxygen isotope effect, and superexchange distribution in La_2CuO_4 . *Phys. Rev. B* **2014**, *89*, 085113. [[CrossRef](#)]
67. Pickett, W.E. Electronic Structure of the High-temperature Oxide Superconductors. *Rev. Mod. Phys.* **1989**, *61*, 433–512. [[CrossRef](#)]
68. Seibold, G.; Lorenzana, J.; Grilli, M. Checkerboard and Stripe Inhomogeneities in Cuprates. *Phys. Rev. B* **2007**, *75*, 100505. [[CrossRef](#)]
69. Okamoto, S.; Furukawa, N. Spontaneous Fourfold-symmetry Breaking Driven by Electron-lattice Coupling and Strong Correlations in High- T_c Cuprates. *Phys. Rev. B* **2012**, *86*, 094522. [[CrossRef](#)]
70. Bersuker, I.B. *Electronic Structure and Properties of Transition Metal Compounds: Introduction to the Theory*; John Wiley & Sons: New York, NY, USA, 2010.

71. Xia, J.; Beyersdorf, P.T.; Fejer, M.M.; Kapitulnik, A. Modified Sagnac interferometer for high-sensitivity magneto-optic measurements at cryogenic temperatures. *Appl. Phys. Lett.* **2006**, *89*, 062508. [[CrossRef](#)]
72. Xia, J.; Schemm, E.R.; Deutscher, G.; Kivelson, S.A.; Bonn, D.A.; Hardy, N.W.; Liang, R.; Siemons, W.; Koster, G.; Fejer, M.M.; et al. Polar Kerr-Effect Measurements of the High-Temperature YBa₂Cu₃O_{6+x} Superconductor: Evidence for Broken Symmetry near the Pseudogap Temperature. *Phys. Rev. Lett.* **2008**, *100*, 127002. [[CrossRef](#)]
73. Li, L.; Alidoust, N.; Tranquada, J.M.; Gu, G.D.; Ong, N.P. Unusual Nernst Effect Suggesting Time-Reversal Violation in the Striped Cuprate Superconductor La_{2-x}Ba_xCuO₄. *Phys. Rev. Lett.* **2011**, *107*, 277001. [[CrossRef](#)]
74. He, R.H.; Hashimoto, M.; Karapetyan, H.; Koralek, J.D.; Hinton, J.P.; Testaud, J.P.; Nathan, V.; Yoshida, Y.; Yao, H.; Tanaka, K.; et al. From a Single-Band Metal to a High-Temperature Superconductor via Two Thermal Phase Transitions. *Science* **2011**, *331*, 1579. [[CrossRef](#)]
75. Harima, N.; Matsuno, J.; Fujimori, A.; Onose, Y.; Taguchi, Y.; Tokura, Y. Chemical potential shift in Nd_{2-x}Ce_xCuO₄: Contrasting behavior between the electron- and hole-doped cuprates. *Phys. Rev. B* **2001**, *64*, 220507. [[CrossRef](#)]
76. Ledbetter, H.; Kim, S.; Roshko, A. Critical-temperature/Debye-temperature correlation in (La-M)₂CuO₄ superconductors. *Phys. C* **1991**, *190*, 129–130. [[CrossRef](#)]
77. Ledbetter, H. Dependence of on Debye temperature OD for various cuprates. *Phys. C* **1994**, *235–240*, 1325–1326. [[CrossRef](#)]
78. Imada, M. Charge Order and Superconductivity as Competing Brothers in Cuprate High-Tc Superconductors. *J. Phys. Soc. Jpn.* **2021**, *90*, 111009. [[CrossRef](#)]